Transcrystallization at the surface of graphene-modified chitosan fibers



2016 J. Phys. D: Appl. Phys. 49 265305

(http://iopscience.iop.org/0022-3727/49/26/265305)

IOP Publishing Journal of Physics D: Applied Physics
J. Phys. D: Appl. Phys. **49** (2016) 265305 (10pp) doi:10.1088/0022-3727/49/26/265305

# Transcrystallization at the surface of graphene-modified chitosan fibers

**Mingxian Liu, Rui He, Jing Yang, Wei Zhao and Changren Zhou**

Department of Materials Science and Engineering, Jinan University, Guangzhou 510632, People's Republic of China

E-mail: liumx@jnu.edu.cn (M Liu)

Received 12 November 2015, revised 17 March 2016
Accepted for publication 29 March 2016
Published 31 May 2016

**Abstract**

Incompatibility between hydrophilic chitosan (CS) fiber and hydrophobic polymer matrices leads to unsatisfactory properties of the composites. The crystallization of polymer on the fiber surface is a promising way to increase interfacial interactions. Here, we coated CS fiber surfaces with graphene oxide via electrostatic self-assembly to improve interfacial interactions between the polymer and the CS fiber. Structures of the CS fiber before and after graphene coating were characterized by various methods. The formation of a polypropylene (PP) transcrystalline (TC) layer on the CS fiber surface was investigated. It is suggested that at low crystallization temperatures the fiber induced TC phase forms faster than at high temperature. There exist $\alpha$ and $\beta$ crystal of PP in the TC phase formation process as demonstrated by x-ray diffraction. The polarized light optical microscope results demonstrate that graphene coated CS fiber can also enhance the TC phase nucleation ability of poly(L-lactide).

Keywords: natural fibers, interface/interphase, optical microscopy, thermal properties

(Some figures may appear in colour only in the online journal)

## 1. Introduction

Fibers reinforced polymer (FRP) composites have many applications in aerospace, leisure, construction, sport, packaging, electronics, and automotive industries [1]. The most commonly used fibers for this purpose are glass fiber, aramid fiber, and carbon fiber. In recent decades, natural polymeric fibers have become attractive as an alternative reinforcement for FRP composites due to their low cost, fairly good mechanical properties, high strength-to-weight ratio, ease of processing, environmental friendliness, and bio-degradability characteristics [2–4]. These natural polymeric fibers can be divided into two types according to their sources. The first type consists of fibers obtained from plant resources, including flax, hemp, jute, sisal, kenaf, coir, kapok, banana, henequen, and many others. The second type consists of fibers derived from animal resources, such as silk, wool, chitin, collagen, and so on [5]. However, incompatibility between hydrophilic polymeric fiber surfaces and hydrophobic polymer matrices always leads to unsatisfactory properties of the FRP composites [2, 6]. It is therefore necessary to modify the fiber surface via physical or chemical routines to improve adhesion between fiber and matrix.

For fiber-reinforced semicrystalline polymer composites, heterogeneous nucleation always occurs with high density along the polymer-fiber interface. This results in crystal growth restricted to the lateral direction, which leads to a columnar layer known as transcrystallinity phase (TC) [7, 8]. The ability to develop TC structure in FRP composites is a new approach to enhancement of interfacial interaction between fillers and polymer matrices. The formation of TC interphase can improve the mechanical properties of FRP composites [9–11]. For example, TC structures in polyethylene (PE) and polypropylene (PP) have higher Young's modulus compared to the spherulites in the bulk [10]. However, the formation mechanism of the TC phase has not been completely understood until now. The fiber material, topology and surface coating, the matrix type and thermal history, as well as other factors, have all been reported to affect TC structure in composites [12–14]. It is likely that the TC layer phenomenon is attributed to unique fiber–matrix interactions.

During the past few decades, chitosan (CS) has attracted much attention and been broadly applied in medical and other areas with respect to its exceptional biological characteristics of unique antiphlogistic effect, bio-compatibility, absorptivity,

 

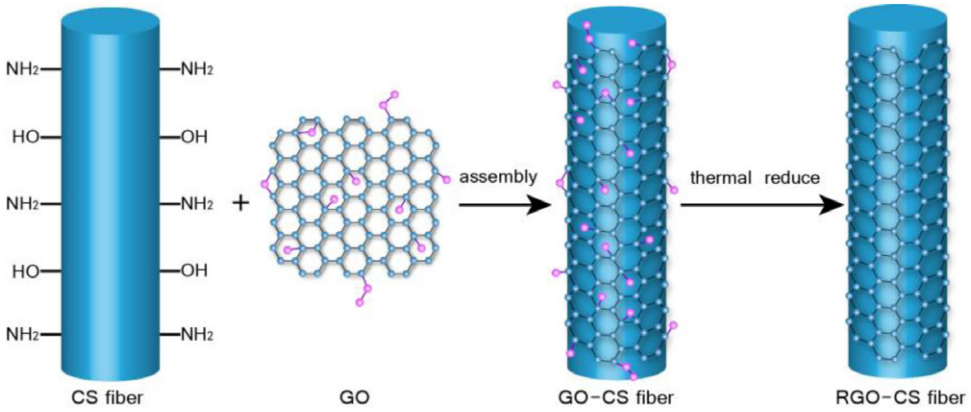


**Figure 1.** Schematic representation of the coating of RGO on CS fiber surface.

non-hypersensitivity, biodegradation property and wound healing [15, 16]. CS can be transformed into microfiber by a wet spinning method [17]. The application of CS fiber is expected in medical areas such as bone setting, human body tissue, medical paper, wound dressing, anti-fungus fabric textile and others [18, 19]. However, the reinforcing ability for FRP composites and TC phase formation ability of CS fiber have not been clear till now. It may be hard to induce polymer TC layer on a raw CS fiber under common crystallization conditions, since the surface structure of CS is irregular. Previous studies show that fiber surface modification by graphene [20] or dopamine [21] could enhance the nucleation ability of fiber on PP and poly(L-lactide) (PLLA) and induce interfacial TC structures. Very recently, graphene-induced oriented interfacial crystals of PP in single fiber polymer composite were examined [14]. Introduction of graphene oxide (GO) to carbon fiber surfaces can also improve the interfacial properties in carbon fiber/epoxy composites [22].

Since CS represents an important biopolymer derived from renewable resources, the research on the properties and application of CS fiber is interesting. In this work, we carried out the coating of GO on CS fiber surfaces via an electrostatic self-assembly process. After the GO was reduced to reduced graphene oxide (RGO), the interfacial crystallization between PP and the graphene coated CS fiber was investigated. Our goal was to find an easy and efficient way to enhance interfacial compatibility between the non-polar PP and polar CS fiber via a physical wrapping method and explore new applications for graphene and CS fiber. The structure of the CS fiber before and after modification, the crystallization behavior of the CS fiber/PP composites, and the formation of TC phase in the composites were investigated. We proposed that coating of RGO on the CS fiber can control the interfacial crystallization of polymer. This technique shows promising applications in polymer/fiber composites with enhanced interfacial interactions and mechanical properties.

## 2. Experimental procedure

### 2.1. Materials

CS fiber with diameter of 20 $\mu$m was purchased from Weifang Youngchito Biochemical Co., Ltd (Shandong, China). GO prepared using Hummers' method [23], and was dried at 60 °C under vacuum for 24 h before use. The GO used had lateral dimension ranging from a few hundred nanometers to several micrometers and an individual sheet thickness of about 1 nm. The C/O atomic ratio of the GO was about 2 by elemental analysis. Isotactic PP (trade name F401), with melt flow index 2.84 g/10 min(after ISO-1133:1997(E)), was purchased from Lanzhou Petro-chemical Co. Ltd, China. PLLA with molecular weight $<M_n> = 1.0 \times 10^6$ was purchased from Huizhou Foryou Medical Device Co., Ltd, China. All other chemicals were analytical grade reagents and were used as received.

### 2.2. Coating of GO on CS fiber surface via sonication assembly strategy

GO aqueous dispersion (1 mg ml$^{-1}$) was prepared via strong ultrasonic treatment using JY99-IIDN ultrasonic cell crusher (Ningbo scientz biotechnology co., LTD, China). Then 3 g CS fiber with a length 30–35 mm was added into the 200 ml GO dispersion. The mixture was ultrasonically treated for 2 h at room temperature to allow the adsorption of GO to the fiber surfaces. Almost all the GO was coated on the surface of CS fibers, as the final GO dispersion became transparent. The fibers were removed from the flask and washed with deionized water several times to remove unbound GO. Then the modified fibers were dried completely under vacuum at 80 °C to obtain GO coated CS fibers (GO-CS). At last, GO absorbed on CS fiber was thermally reduced under vacuum at 150 °C for 2 h to obtain RGO coated CS fiber (RGO-CS). 150 °C was selected as the thermal reduction temperature of GO-CS fiber since thermal decomposition of the CS took place upon heating to 200 °C [24].

### 2.3. Characterization

Scanning electron microscopy (SEM) images of the morphologies of CS fiber before and after coating were observed with a ZEISS Ultra55 SEM at an accelerating voltage of 5 kV. Raman spectra of the fibers were obtained using a multichannel confocal micro spectrometer with a laser wavelength of 535 nm. The melting curves of the fibers were recorded by differential scanning calorimetry (DSC) TA Q20 at the rate of 10 °C min$^{-1}$ under nitrogen atmosphere. Thermogravimetric

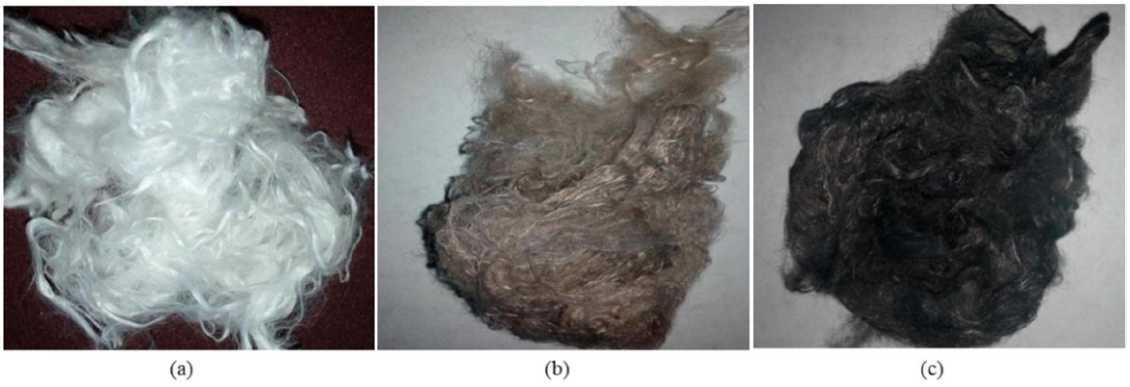


**Figure 2.** Images of raw CS fiber (a), GO-CS fiber (b), and RGO-CS fiber (c).

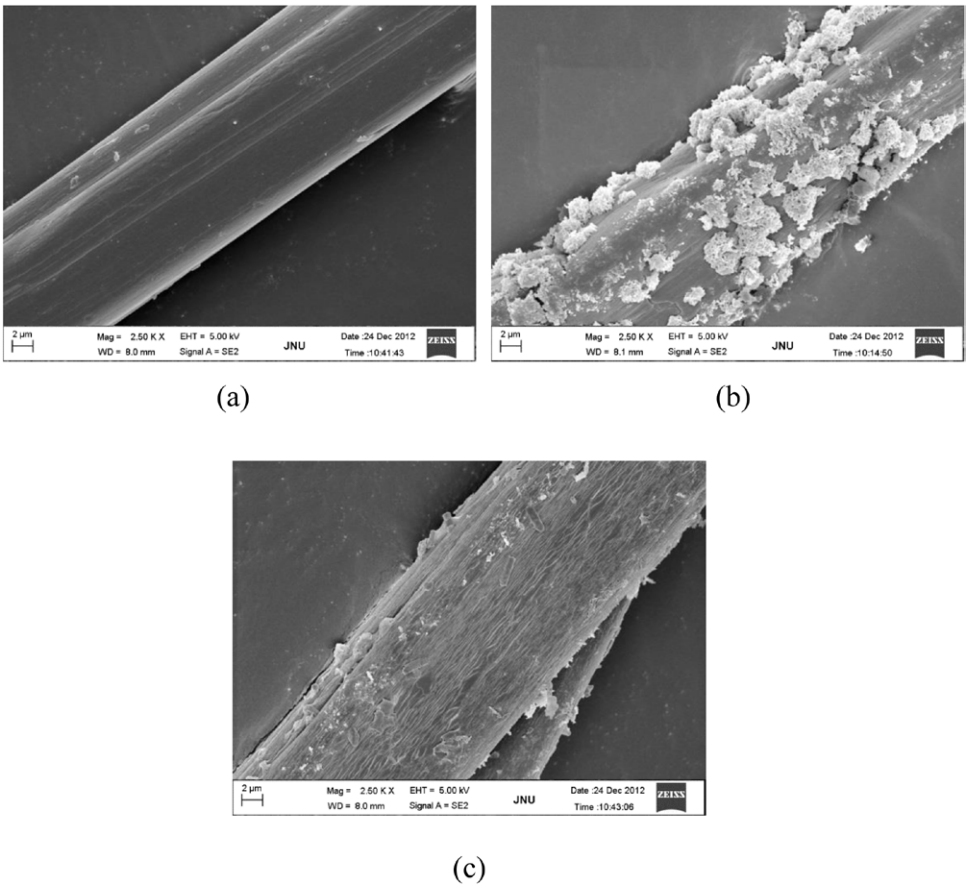


**Figure 3.** SEM morphology of raw CS fiber (a), GO-CS fiber (b), RGO-CS fiber (c).

analysis (TGA) of the fibers was carried out with TA Q5000 from room temperature to 600 °C at a heating rate of 10 °C $min^{-1}$ under $N_2$ atmosphere. X-ray photoelectron spectroscopy (XPS) spectra of the fibers were recorded by a Thermo-VG Scientific ESCALAB 250 with an aluminum (mono) K$\alpha$ source (1486.6 eV). The Al K$\alpha$ source was operated at 15 kV and 10 mA. The fiber/PP composites were prepared by melting mixing in a Labo Plastomill $\mu$ torque rheometer at 170 °C. X-ray diffraction (XRD) patterns of PP and the CS fiber/PP composites were recorded using a Rigaku MiniFlex600 x-ray diffractometer. The CuK$\alpha$ radiation source was operated at 40 kV power and 40 mA current. Patterns were recorded by monitoring those diffractions that appeared from 5 to 50°. The scanning speed was 4° $min^{-1}$. XRD samples were prepared by hot-pressing at 180 °C and subsequently cooling to room temperature. A polarized light optical microscope (PLM) equipped with a hot stage was used to study the nucleation ability and crystallization morphology of CS fiber or RGO-CS fiber in PP crystallization. Samples sandwiched between two microscope cover slips were first heated to 200 °C, pressed into thin films, and then maintained at 200 °C for 5 min to erase any thermal history. The temperature of the hot stage was then reduced to the fixed crystallization temperature ($T_c$) at a rate of 10 °C $min^{-1}$. The crystallization process was observed and the morphologies were recorded by taking photographs. The melting of the TC layer formed was effected by heating the

RGO-CS/PP composite sample at a rate of 5 °C $min^{-1}$. DSC data of the PP and CS fiber/PP composites were measured by a TA Q20 using nitrogen as purging gas. Samples were heated to 200 °C at the ramping rate of 40 °C $min^{-1}$. Each sample was kept at 200 °C for 3 min to eliminate thermal history before it was cooled down to 40 °C at the rate of 10 °C $min^{-1}$. The second endothermic and exothermic flows were recorded as a function of temperature.

## 3. Results and discussions

### *3.1. Coating of GO on CS fiber surface via electrostatic self-assembly*

The amino groups of the CS make it positively charged, whereas GO sheets are negatively charged due to the presence of oxygen functional groups such as phenolic hydroxyls and carboxylic acids. By simply mixing the aqueous suspension of CS fiber and GO colloid solution, GO can be satisfactorily coated onto the positively charged CS fiber surface via an electrostatic self-assembly process. To change the amorphous GO coated CS fiber surface into crystalline graphite surface, the fiber is kept at 150 °C for 2 h for reduction of the GO. The coating process of graphene on CS fiber surface via electrostatic self-assembly and subsequent reduction is illustrated in figure 1.

The appearance of the raw CS fiber, GO-CS fiber, and RGO-CS fiber is shown in figure 2. It can be seen that the white color of the original CS fibers changes to brown after coating of the GO on their surfaces. Homogeneous staining of the CS fiber by GO indicates successful wrapping of the GO on the fiber. After reduction of GO by heat treatment, the brown-colored GO-CS fibers turn black. SEM observation and Raman spectroscopy results further confirm the coating of graphene on the CS fibers. Raw CS fiber has a relatively smooth surface, as shown in figure 3(a). After electrostatic self-assembly of GO, the fiber surfaces are coated with the flower-like GO sheet aggregate. By thermal reduction of the GO-CS fiber, an ultrathin and uniform film of RGO sheet is found on the fiber surface with wrinkled and roughened textures. The formation of GO bulk aggregates on the CS fiber surface is attributed to the hydrogen bonding interactions between the epoxy and hydroxyl functional groups on individual GO platelets at high GO dispersion concentration [25]. After thermal reduction, the hydrogen bonding interactions between the sheets decrease due to the decreased oxygen atom content—so a relatively uniform film of RGO is found on the fiber surface. The adhesion of GO sheet on the fiber is attributed to the hydrogen bonding and the Van der Waals' force. Similar results have also been found in graphene coated glass fiber systems [20]. All these results suggest that RGO has been successfully coated on CS fiber surface.

Raman spectroscopy is a powerful tool for the characterization of carbon nanostructures. We employed Raman technique to further demonstrate the successful coating of RGO on CS fiber surfaces. The comparison of Raman spectra of the CS fiber, GO-CS fiber, and the RGO-CS fiber is shown in figure 4. For RO-CS fiber and RGO-CS fiber, two typical peaks

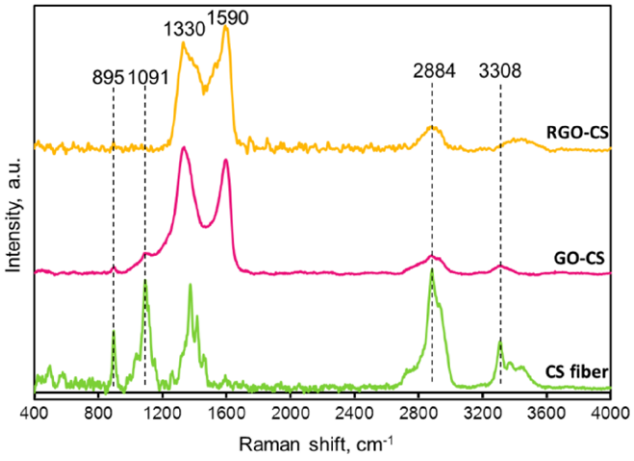


**Figure 4.** Raman spectra of raw CS fiber, GO-CS fiber, and RGO-CS fiber.

at 1330 (D band) and 1590 $cm^{-1}$ (G band) can also be clearly observed, corresponding to the disordered structure of the graphene sheets and high-frequency $E_{2g}$ Raman scattering mode of $sp^2$-hybridized carbon respectively [26, 27]. The bands at 2884 and 3308 $cm^{-1}$, representing the stretching vibrations of C–H and N–H groups of CS, decreased in the GO-CS fiber and RGO-CS fiber samples [28]. The peaks around 895 and 1091 $cm^{-1}$, attributed to symmetric stretching of glycosidic bonds (–C–O–C–) and $NH_2$ wagging in CS backbones, respectively [28–30], decrease in the GO-CS fiber and totally disappear in the RGO-CS fiber. The signals assigned to CH bending, $CH_2$ wagging, $CH_2$ twisting, and $CH_3$ bending, lying in the range of 1200 and 1415 $cm^{-1}$ of CS, are overlapped with the D band of the graphene [28, 30]. The 2D peak of graphene (always located around 2700 $cm^{-1}$) is hardly found in the GO-CS and RGO-CS fiber samples, which may be due to the overlap of the peak with the 2888 $cm^{-1}$ peak of CS. In addition, the intensity of the 2D-band with respect to the D and G peaks is low [31]. Therefore, the Raman spectra results also indicate that graphene is successfully coated onto the CS fiber surface.

The RGO layer on the outer surface of CS fibers can improve the thermal degradation stability of the CS, as the graphene sheets can protect the polymer from the attack by heat. DSC and TGA were utilized to investigate the thermal stability of CS before and after RGO coating. From figure 5(a), no apparent thermal signals around 190 °C attributed to the thermal reduction of GO are observed for GO-CS fiber sample [32], which is due to the low content of GO in the GO-CS fiber. The thermal transition temperature of the RGO-CS fiber determined by DSC is increased to 117.2 °C, which is 5.6 °C higher than that of the raw CS fiber. TGA and differential thermogravimetric analysis (DTG) results (figure 5(b)) also show the degradation temperature of the RGO-CS fiber is 17 °C higher than that of the CS fiber. The peak of weight loss around 64 °C and 280 °C of CS is assigned to the loss of adsorbed water and degradation of the CS chains respectively [5]. The enhancement of thermal stability of CS by GO coating is attributed to the layered structure and high thermal stability of graphene. The wrapping of high heat resistant

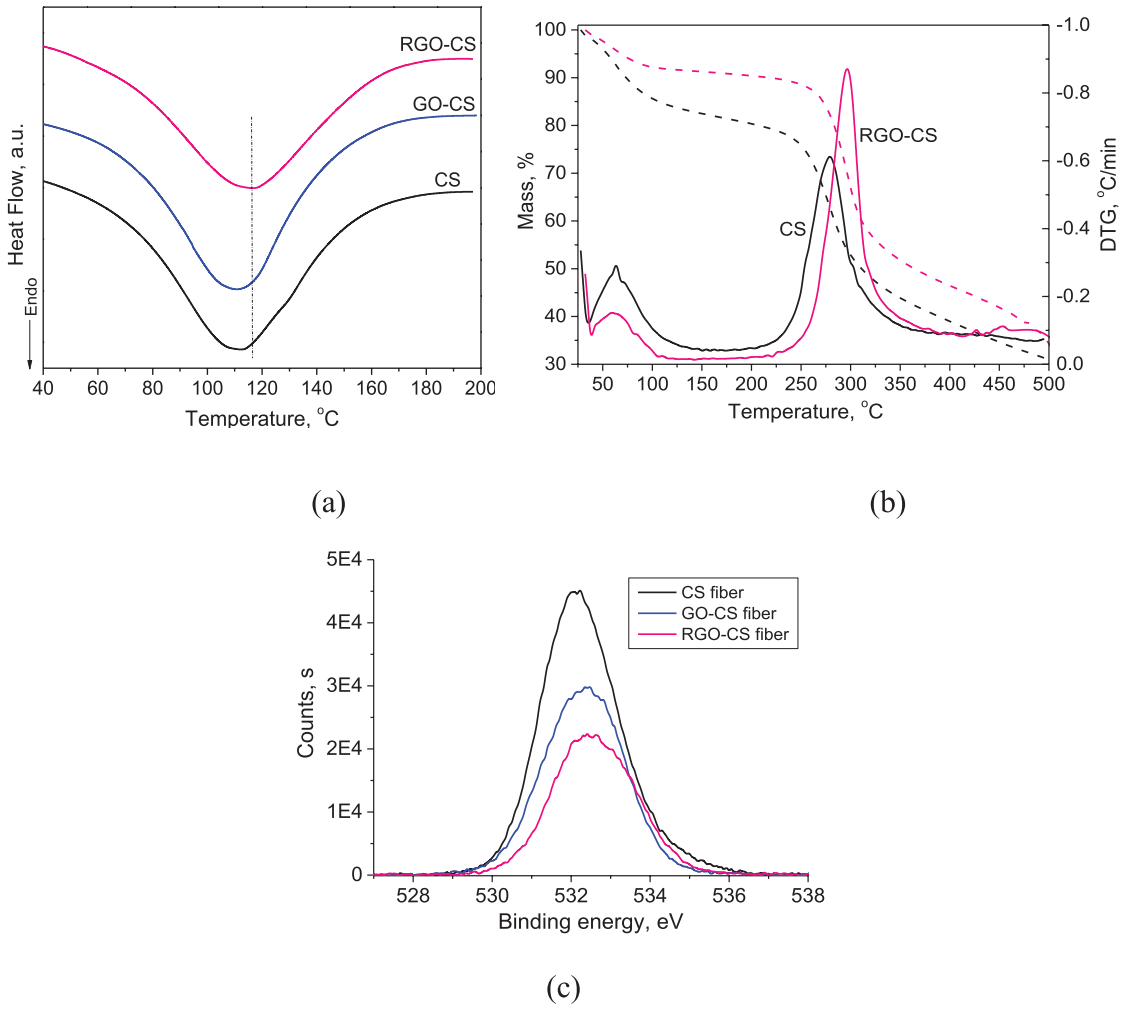


**Figure 5.** DSC curve (a), TGA thermograms (b), and XPS O1s scan (c) of raw CS fiber, GO-CS fiber, and RGO-CS fiber (the solid line in (b) represents DTG curve).

graphene was also found to increase the thermal stability of polymersin previous studies [33]. Therefore, from the thermal analysis results, graphene sheets are successfully coated on the CS fiber, which results in improved thermal stability of the CS fiber.

XPS analysis was further conducted to study the chemical composition of the three fiber samples. Figure 5(c) shows the $O_{1s}$ spectrum for the raw CS fiber, GO-CS fiber, and RGO-CS fiber. It can be seen that the peak intensity of $O_{1s}$ of the CS fiber decreases via the GO coating. This is because the oxygen content in GO is less than that in CS. Upon thermal reduction, the $O_{1s}$ peak value decreases further, which is attributed to the transformation of the GO to RGO. Table 1 summarizes the atomic concentration (at.%) of $C_{1s}$ and $O_{1s}$ and the C/O atomic ratio of the fiber samples. The increase in C/O ratio of the modified fiber can also be interpreted as a result of coating GO onto the CS fiber surface. The RGO-CS fiber has the highest C/O atomic ratio (1.92), which indicates the successful reduction of the GO during the heating treatment at 150 °C. The inconsistent C/O atomic ratio of the raw CS fiber (0.57) and previously reported CS powder (0.5) may come from the impurity of the CS fiber during the preparation process [34, 35]. It should be noted that the oxygen in the RGO-CS fiber is ascribed to the bare CS fiber surface and the non-reduced GO. The wrapping of the graphene sheets on the CS fiber may not be complete as shown in the SEM and Raman spectra results. Also, the relatively low reduction temperature leads to a low reduction ratio of GO [32, 33]. However, the RGO-CS fiber prepared using this strategy is already effective for inducing the interfacial crystallization of polymers, which will be shown in the following sections.

**Table 1.** XPS atomic content (at.%) and C/O atomic ratio for raw CS fiber, GO-CS fiber, and RGO-CS fiber.

| Sample | C | O | C/O ratio |
|---|---|---|---|
| Raw CS fiber | 27.51 | 48.56 | 0.57 |
| GO-CS fiber | 54.34 | 34.63 | 1.57 |
| RGO-CS fiber | 58.57 | 30.47 | 1.92 |

In brief, graphene has been successfully coated on the CS fiber surface via an electrostatic self-assembling strategy, which obviously changes the surface topography structure of the fiber, and also changes the fiber surface into crystalline graphite surface after thermal reduction. The RGO-CS fiber so obtained exhibits increased thermal stability compared with the original CS fiber. RGO-CS fibers will be used as

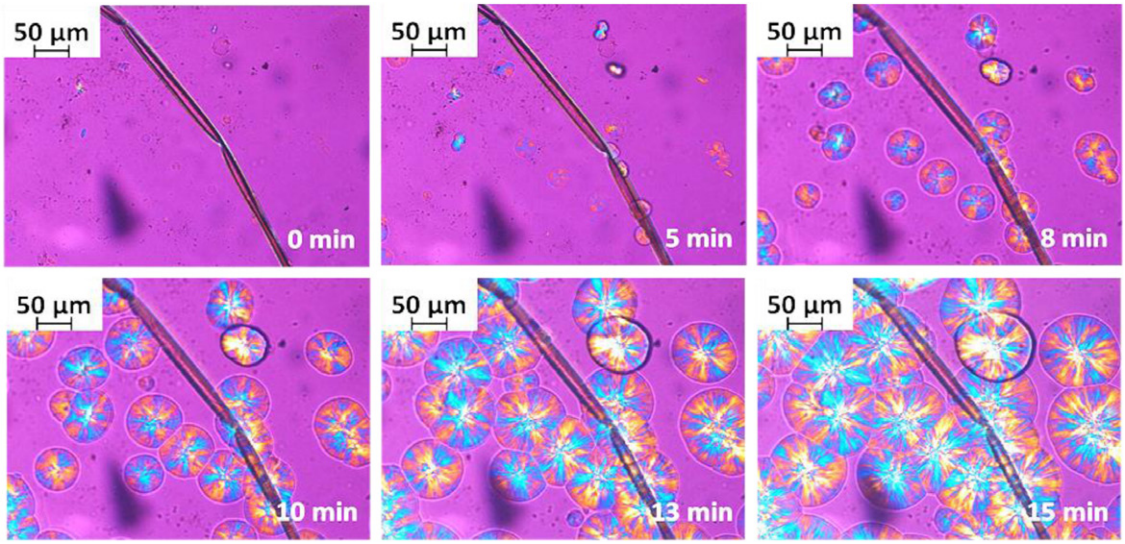


**Figure 6.** Optical micrographs of crystalline interphases for CS/PP crystallized at 138°C.

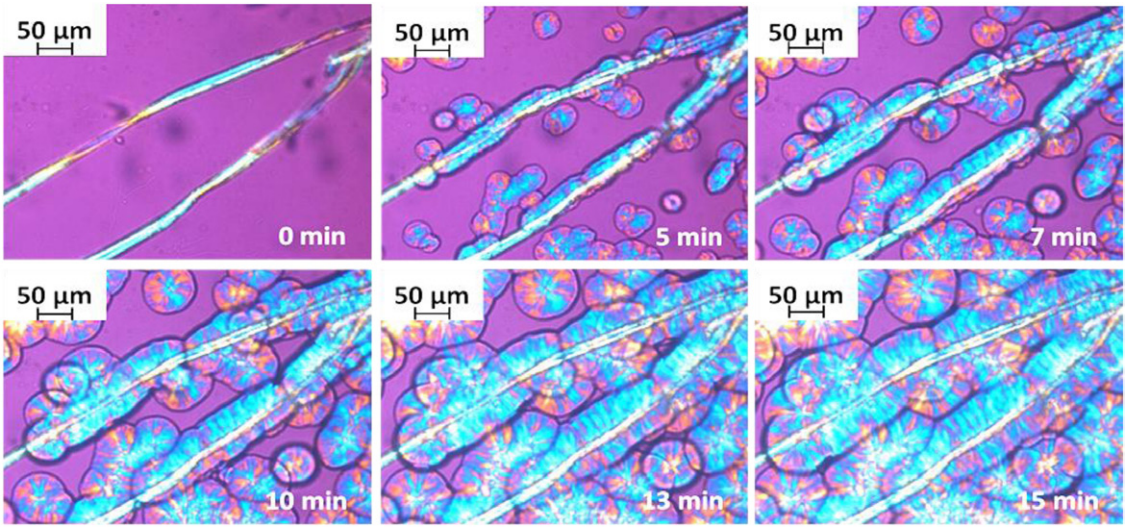


**Figure 7.** Optical micrographs of crystalline interphases for RGO-CS fiber/PP composite crystallized at 135 °C.

nucleating agent to induce interfacial TC structures in semicrystalline PP or PLLA.

### *3.2. RGO-CS fiber induced TC phase of PP*

The crystallization process of unmodified CS fiber/PP composite and RGO-CS fiber/PP composite was monitored by PLM. For raw CS fiber composite, no TC layer is found on the fiber surface, but spherulites are clearly observed in the bulk, as shown in figure 6. Thus, raw CS fiber has almost no nucleation ability on PP crystallization. Figures 7–9 show a series of optical images of the RGO-CS fiber/PP composite taken at 135, 138, and 141 °C respectively with different crystallization times. The RGO-CS fiber induces a dense population of PP crystal nuclei along its surface, which leads to oriented growth of the PP lamellae away from the fiber outward into the matrix, thus forming a TC layer. Away from the RGO-CS fiber, spherulites are also found. The formation process of the TC layer is more or less similar for samples crystallized at different temperatures, and not much difference can be detected from the appearance of morphology. However, if the growth rate is compared for these systems, one can see that the thickness of the TC layer is larger and the density of nuclei higher at low crystallization temperature than at high crystallization temperature in the same crystallization time.

From the formation process of TC structure at RGO-CS fiber/PP interface, one can clearly observe that numerous nuclei are induced on RGO-CS fiber surface. The nuclei grow perpendicular and parallel to the long axis of fiber, and gradually impinge with each other with increasing crystallization time. Finally, TC structures along the fiber surfaces are successfully obtained. These results suggest that coating of graphene sheets on the CS fiber surface can greatly improve the nucleation ability of CS fiber for PP crystallization and thus induce the formation of TC structures. RGO coated glass fiber, dopamine treated ramie fiber, and graphene fibers have also been found to have the ability of induction of TC structures in PP or PLLA [6, 20, 21].

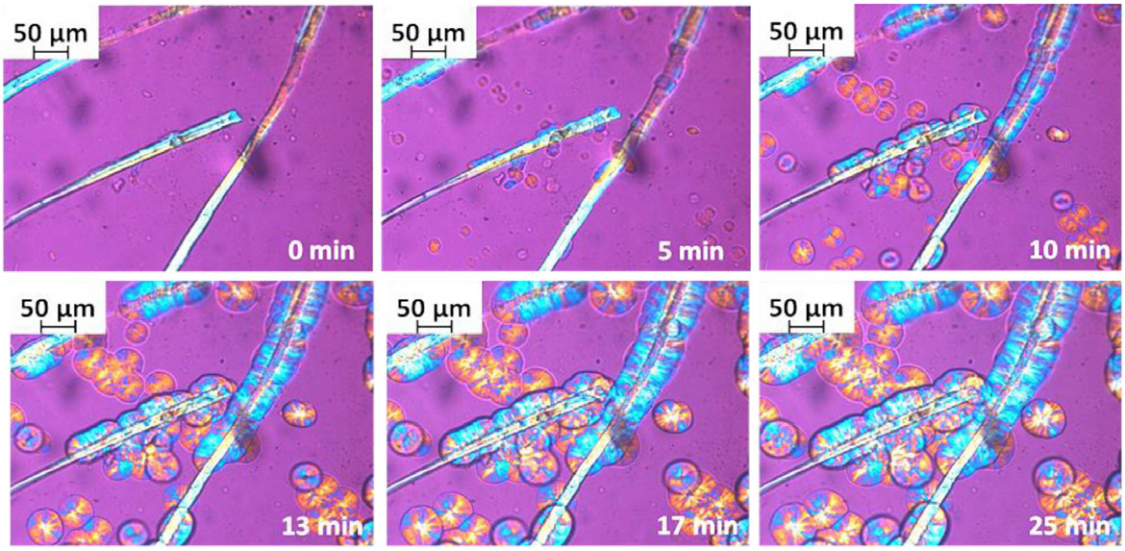


**Figure 8.** Optical micrographs of crystalline interphases for RGO-CS fiber/PP composite crystallized at 138 °C.

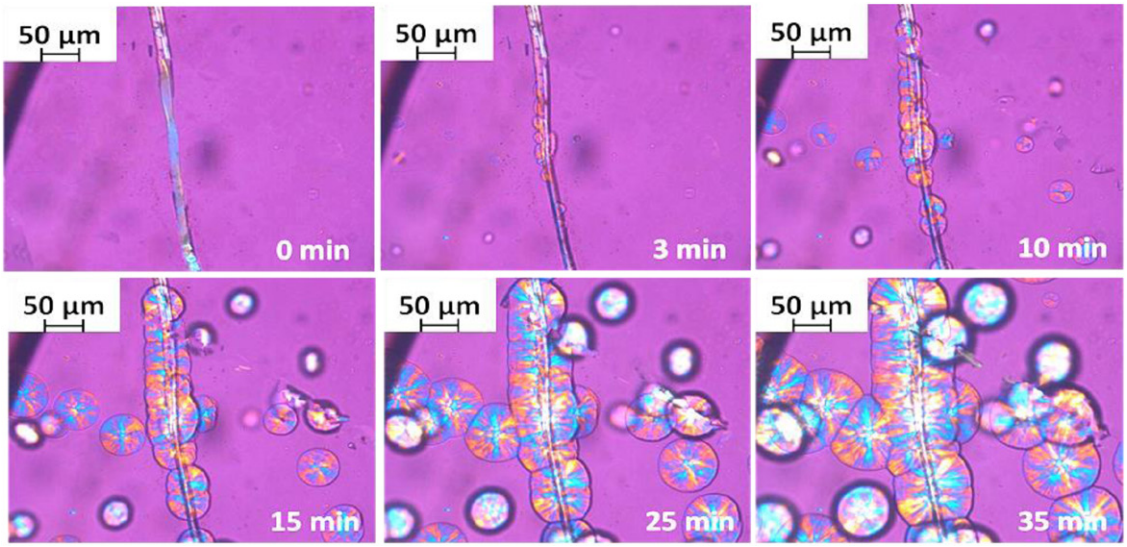


**Figure 9.** Optical micrographs of crystalline interphases for RGO-CS fiber/PP composite crystallized at 141 °C.

Crystallization kinetics of the TC phase was further investigated for the RGO-CS fiber/PP composites. Figure 10 displays the relationships between TC layer thickness and crystallization time of the RGO-CS fiber/PP composite. Each curve exhibits a sigmoid dependent on crystallization time. The time to reach the TC phase thickness 'plateau', which means the TC phase developed completely, is reduced to 15 min at the crystallization temperature of 135 °C, while the time to the 'plateau' is 45 min for the same sample crystallized at 141 °C. The growth rate of the TC phase increases with the decrease of the crystallization temperature. This arises from the fact that the driving force of the TC phase formation increases as the sample is supercooled which is consistent with previous study [8].

RGO-CS fiber can also promote the formation of TC structure of PLLA as shown in figure 11. From figure 11(a), one can see that several sporadic spherulites of PLLA only appear on the surface and the cross points of CS fibers while

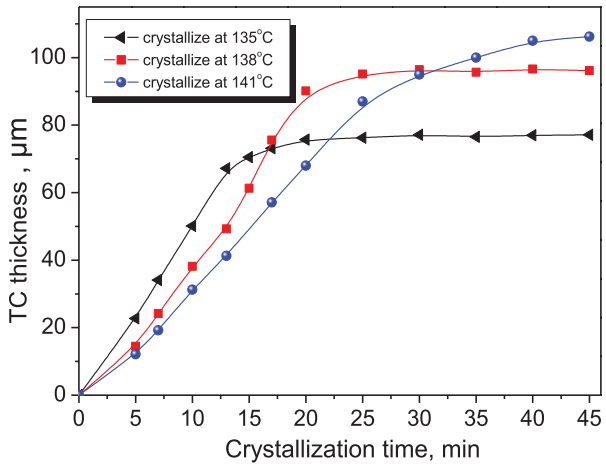


**Figure 10.** Growth of TC layer thickness of RGO-CS fiber/PP composite as a function of time.

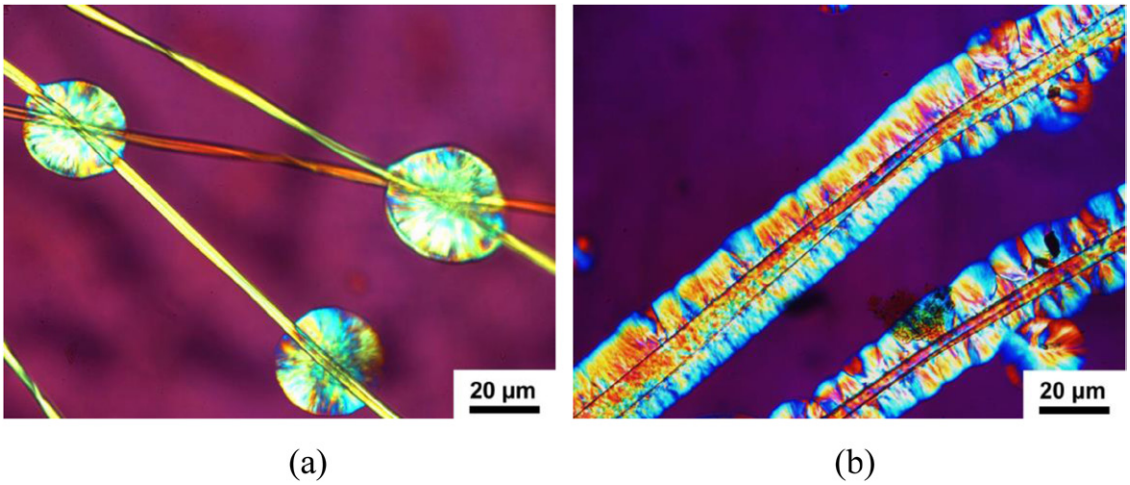


**Figure 11.** Optical micrographs of crystalline interphases for CS fiber/PLLA (a) and RGO-CS fiber/PLLA (b) composite isothermally crystallized at 145 °C.

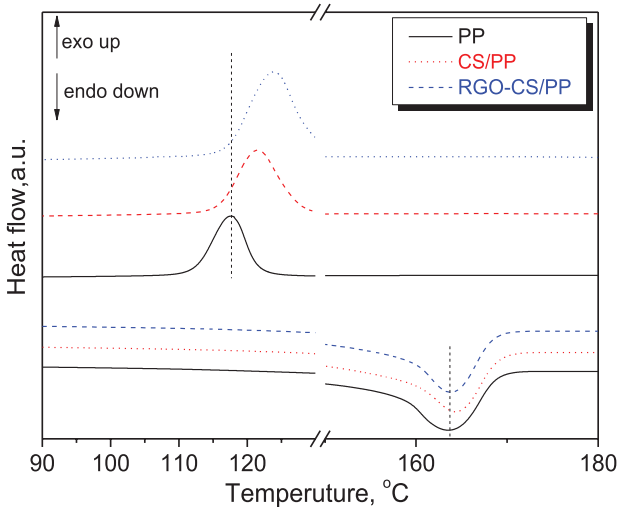


**Figure 12.** DSC heating and cooling curves thermograms of PP, CS fiber/PP composite, and RGO-CS fiber/PP composite.

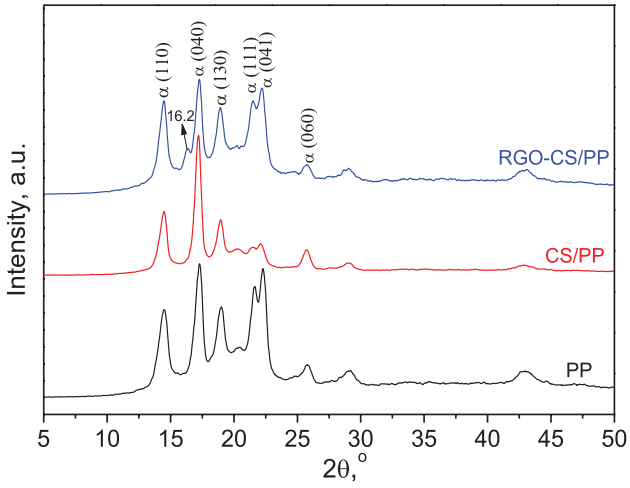


**Figure 13.** XRD spectra of PP, CS fiber/PP composite, and RGO-CS fiber/PP composite.

no spherulites can be found in the PLLA matrix. So, raw CS fiber has weak nucleation ability for PLLA crystallization. For RGO-CS fiber, perfect TC structure is formed on the fiber surface. This suggests again obviously enhanced nucleation ability of RGO-CS fiber for PLLA crystallization. These results are in agreement with the previous report by Fu *et al* [20].

As observed in the PLM photos, the nucleation density on RGO-CS fiber surface is not high enough, which leads to the possibility that the crystallites could develop in two directions (perpendicular and parallel to the long axis of the fiber surface) prior to the formation of TC structure. This kind of TC structure is called medium density TC [20]. If there are enough active points on the fiber surface, this hinders a full extension of spherulites and forces crystal growth only in one direction. The concentration and reduction degree of GO can be changed to tailor the nucleation density to obtain different types of interfacial crystallization structure of polymer. These will be conducted in our future work. In any case, these results demonstrate that the coating of RGO could effectively improve the nucleation ability of CS fiber on PP and PLLA crystallization, and thus largely enhance the interfacial TC structures of polymers on CS fiber surfaces. This could be explained by the following two reasons: chemical composition changes and morphology changes. Chemically, the CS fiber surface transforms into the crystalline graphite surface after coating with RGO, which can facilitate the formation of an oriented structure of polymer chains due to the chemisorptions of macromolecular chains on RGO. Morphologically, the wrinkled and rough texture of RGO on CS fiber surfaces obviously changes the surface topography structure of the fiber. As suggested by Fu *et al* [20], the 'groove structure' on the fiber surface facilitates the orientation of polymer chains along the 'groove' and the lateral formation of a stable nucleus.

### *3.3. Crystallization structure of CS fiber/PP composites*

Figure 12 shows the DSC heating and cooling curves of PP and the CS fiber/PP composites. For pure PP, an exothermic peak occurs at $T_c = 117.7$ °C in the cooling curve. For CS fiber/PP and RGO-CS fiber/PP composites, the exothermic peaks shift to $T_c = 121.6$ and 123.8 °C respectively. Due to the

fact that the addition of the fibers does not affect the molecular weight or cause chain branching of PP, which might impact the crystalline phase of PP in the composites, only the nucleating activity of the fibers is to be considered. Therefore, the observed effects can be ascribed to the rapid crystallization rate of the composite and the nucleating effect of the fibers in the PP crystallization process [32]. All the samples exhibit a single endothermic peak at around 163.7 °C in the heating curve, indicating the fibers have no effect on the melting behavior. The nanoparticles in the polymer matrix always induce the shift of $T_c$ to higher temperature due to the small size effect [36, 37].

XRD was further employed to investigate the crystal structure of the CS fiber/PP composites. Figure 13 shows the XRD patterns of the non-isothermally crystallized CS fiber/PP composites. The peaks at diffraction angles $2\theta$ of 14.2, 17.1, 18.7, 21.1, and 22.2° are attributed to (1 1 0), (0 4 0), (1 3 0), (1 1 1) and (0 4 1) reflections respectively, which are based on the $\alpha$-form monoclinic packing of PP [38, 39]. Consistent with the results from DSC, the unmodified CS fiber has no nucleating effect on the PP. The RGO-CS/PP composites exhibit a new peak around 16.2° assigned to the $\beta$(3 0 0) [40]. This suggests that RGO-CS fiber induces the $\beta$-crystal of PP during the crystallization process. Other fibers such as PET fiber [41] and ramie fiber [21] can also induce $\beta$-PP lamellar crystals on their surfaces.

## 4. Conclusions

GO was successfully coated onto the positively charged CS fiber surface via an electrostatic self-assembly method. RGO-CS fibers exhibit wrinkled and roughened surface textures and improved thermal stability compared to raw CS fiber. No TC layer of PP is found on the fiber surface for raw CS fiber. RGO-CS fiber can greatly improve the nucleation ability of CS fiber for PP crystallization and induce the formation of TC structure. The growth of the TC layer is a function of the crystallization temperature and the crystallization time. There exist $\alpha$ and $\beta$ crystal forms of PP in the TC phase formation process. RGO-CS fiber can also induce the formation of a TC phase in PLLA. These results provide guidance for the preparation of polymer/natural fiber composites with enhanced interfacial interactions via the formation of TC layers using simple surface modification. The mechanism of the formation of the TC phase and better controlling the formation of TC structure for improving the interfacial adhesion of polymer/CS fiber composites will be conducted in our future work.

## Acknowledgments

This work was financially supported by the National Natural Science Foundation of China (grant No. 51473069 and 51502113) and the Guangdong Natural Science Funds for Distinguished Young Scholars (grant No. S2013050014606), the Special Fund for Ocean-Scientific Research in the public interest (201405105), and the Fundamental Research Funds for the Central Universities (21615204).

## References

[1] Bakis C *et al* 2002 Fiber-reinforced polymer composites for construction-state-of-the-art review *J. Compos. Constr.* **6** 73–87
[2] Ku H *et al* 2011 A review on the tensile properties of natural fiber reinforced polymer composites *Compos.* B **42** 856–73
[3] Holbery J and Houston D 2006 Natural-fiber-reinforced polymer composites in automotive applications *JOM* **58** 80–6
[4] Malkapuram R, Kumar V and Negi Y S 2009 Recent development in natural fiber reinforced polypropylene composites *J. Reinf. Plast. Compos.* **28** 1169–89
[5] Neto C G T *et al* 2005 Thermal analysis of chitosan based networks *Carbohydr. Polym.* **62** 97–103
[6] Thwe M M and Liao K 2003 Durability of bamboo-glass fiber reinforced polymer matrix hybrid composites *Compos. Sci. Technol.* **63** 375–87
[7] Schoolenberg G E and Van Rooyen A A 1993 Transcrystallinity in fiber-reinforced thermoplastic composites *Compos. Interf.* **1** 243–52
[8] Wang C and Hwang L M 1996 Transcrystallization of PTFE fiber/PP composites (I) crystallization kinetics and morphology *J. Polym. Sci.* B **34** 47–56
[9] Zhang S *et al* 2008 Polymer transcrystallinity induced by carbon nanotubes *Polymer* **49** 1356–64
[10] Kwei T K, Schonhorn H and Frisch H L 1967 Dynamic mechanical properties of the transcrystalline regions in two polyolefins *J. Appl. Phys.* **38** 2512–6
[11] Wang C and Hwang L M 1996 Transcrystallization of PTFE fiber/PP composites. II. Effect of transcrystallinity on the interfacial strength *J. Polym. Sci.* B **34** 1435–42
[12] Zafeiropoulos N E *et al* 1999 Characterisation of LDPE residual matrix deposited on glass fibres by a dissolution/reprecipitation recycling process *Composites* A **30** 831–8
[13] Zafeiropoulos N E, Baillie C A and Matthews F L 2001 A study of transcrystallinity and its effect on the interface in flax fibre reinforced composite materials *Composites* A **32** 525–43
[14] Abdou J P *et al* 2015 Graphene-induced oriented interfacial microstructures in single fiber polymer composites *ACS Appl. Mater. Interfaces* **7** 13620–6
[15] Shigemasa Y and Minami S 1996 Applications of chitin and chitosan for biomaterials *Biotechnol. Genet. Eng. Rev.* **13** 383–420
[16] Singla A and Chawla M 2001 Chitosan: some pharmaceutical and biological aspects—an update *J. Pharm. Pharmacol.* **53** 1047–67
[17] East G C and Qin Y 1993 Wet spinning of chitosan and the acetylation of chitosan fibers *J. Appl. Polym. Sci.* **50** 1773–9
[18] Tuzlakoglu K *et al* 2004 Production and characterization of chitosan fibers and 3D fiber mesh scaffolds for tissue engineering applications *Macromol. Biosci.* **4** 811–9
[19] Zhang X *et al* 2007 *In vitro* degradation and biocompatibility of poly(l-lactic acid)/chitosan fiber composites *Polymer* **48** 1005–11
[20] Ning N *et al* 2013 Largely enhanced crystallization of semi-crystalline polymer on the surface of glass fiber by using graphene oxide as a modifier *Polymer* **54** 303–9
[21] Zhou M *et al* 2014 Transcrystalline formation and properties of polypropylene on the surface of ramie fiber as induced by shear or dopamine modification *Polymer* **55** 3045–53
[22] Zhang X *et al* 2012 Interfacial microstructure and properties of carbon fiber composites modified with graphene oxide *ACS Appl. Mater. Interfaces* **4** 1543–52
[23] Hummers W S Jr and Offeman R E 1958 Preparation of graphitic oxide *J. Am. Chem. Soc.* **80** 1339

[24] Zawadzki J and Kaczmarek H 2010 Thermal treatment of chitosan in various conditions *Carbohydr. Polym.* **80** 394–400
[25] Medhekar N V *et al* 2010 Hydrogen bond networks in graphene oxide composite paper: structure and mechanical properties *ACS Nano* **4** 2300–2306
[26] Vidano R and Fischbach D B 1978 New lines in the Raman spectra of carbons and graphite *J. Am. Ceram. Soc.* **61** 13–7
[27] Cançado L G *et al* 2011 Quantifying defects in graphene via Raman spectroscopy at different excitation energies *Nano Lett.* **11** 3190–6
[28] Zhang K *et al* 2010 NMR and FT Raman characterisation of regioselectively sulfated chitosan regarding the distribution of sulfate groups and the degree of substitution *Polymer* **51** 4698–705
[29] Monti P *et al* 2005 Structure modifications induced in silk fibroin by enzymatic treatments. A Raman study *J. Mol. Struct.* **744–7** 685–90
[30] Orrego C E *et al* 2010 Novel chitosan membranes as support for lipases immobilization: characterization aspects *Carbohydr. Polym.* **79** 9–16
[31] Yang D *et al* 2009 Chemical analysis of graphene oxide films after heat and chemical treatments by x-ray photoelectron and micro-Raman spectroscopy *Carbon* **47** 145–52
[32] Mi Y, Chen X and Guo Q 1997 Bamboo fiber-reinforced polypropylene composites: crystallization and interfacial morphology *J. Appl. Polym. Sci.* **64** 1267–73
[33] Du J and Cheng H M 2012 The fabrication, properties, and uses of graphene/polymer composites *Macromol. Chem. Phys.* **213** 1060–77
[34] Amaral I, Granja P and Barbosa M 2005 Chemical modification of chitosan by phosphorylation: an XPS, FT-IR and SEM study *J. Biomater. Sci., Polym. Ed.* **16** 1575–93
[35] Vieira R S *et al* 2011 Copper, mercury and chromium adsorption on natural and crosslinked chitosan films: an XPS investigation of mechanism *Colloids Surf.* A **374** 108–14
[36] Anoop Anand K, Agarwal U S and Joseph R 2006 Carbon nanotubes induced crystallization of poly(ethylene terephthalate) *Polymer* **47** 3976–80
[37] Liu M *et al* 2009 Halloysite nanotubes as a novel $\beta$-nucleating agent for isotactic polypropylene *Polymer* **50** 3022–30
[38] Cho K *et al* 2002 Real time *in situ* x-ray diffraction studies on the melting memory effect in the crystallization of $\beta$-isotactic polypropylene *Polymer* **43** 1407–16
[39] Varga J and Karger-Kocsis J 1994 The difference between transcrystallization and shear-induced cylindritic crystallization in fibre-reinforced polypropylene composites *J. Mater. Sci. Lett.* **13** 1069–71
[40] Li J, Cheung W and Jia D 1999 A study on the heat of fusion of $\beta$-polypropylene *Polymer* **40** 1219–22
[41] Sun X *et al* 2007 Alfa and beta interfacial structures of the iPP/PET matrix/fiber systems *Macromolecules* **40** 8244–9